subfragments,[51c] exchange-coupling interactions will also follow the magnetostructural relationship described by eq 2. This type of "magnetic dissection" using the HDVV formalism has been proposed previously for oxo-bridged trinuclear $Fe^{III}_2Mn^{II}$ complexes, but only recently have inelastic neutron scattering studies confirmed its validity.[31b]

The remaining entries in Table III are predictions based on structural data for planar $\{Fe_4O_2\}$ cores (entries 1 and 2), an adamantane-like arrangement of a $\{Fe_4O_4\}$ core (entry 4), and three $\{Fe_2O\}_2$ cores that are so far apart that the "interdimer" interactions are negligible (entries 5, 6, and 8). The calculated $P$ and $J$ values are also listed for these incompletely characterized complexes. For entry 7 the agreement is also reasonable, especially for the shorter $P$. It will be interesting to determine the highest degree of nuclearity of iron oxo aggregates for which the magnetostructural correlation is valid. The answer may shed light on the problem of determining the borderline between a molecular structure, described by localized, pairwise magnetic interactions, and a solid-state structure, described by extended, long-range interactions.

Data on metalloenzymes known or believed to contain dinuclear iron(III) oxo centers are presented in Table IV. Exchange-coupling constants of $-150$ and $-120$ $cm^{-1}$, are predicted for azidomethemerythrin and azidometmyohemerythrin, respectively. These values are in good agreement with those determined for hemerythrin models.

The $-77$-$cm^{-1}$ value of oxyhemerythrin approaches the $-55$-$cm^{-1}$ value obtained for the "intradimer" coupling in $[Fe_3O(TIEO)_2(O_2CPh)_2Cl_3]$. In this complex the Fe–O–Fe unit is "metalated" but the third $Fe^{3+}$ is not as close to the $\mu_2$-oxo atom as it is in basic iron carboxylates and sulfates, $-J = 26$–$31$ $cm^{-1}$. A hydrogen bond to the $\mu$-oxo atom of oxyhemerythrin is therefore reasonable since it will lengthen the Fe–O distance, thus making it intermediate between a $\mu$-oxo and a $\mu$-hydroxo bond ($J = 7$–$11$ $cm^{-1}$ for hydroxo-bridged complexes). The presence of a hydrogen-bonded hydroperoxide group[8c] at the active site of oxyhemerythrin is thus entirely consistent with the magnetic results, and the iron–oxo bond is predicted to be 1.829 Å long. This value is in excellent agreement with the 1.82-Å Fe–O bond length measured by EXAFS.[44b]

For ribonucleotide reductase a $P$ value of 1.80 ± 0.02 Å is predicted, in agreement with a recent EXAFS determination.[55] Uteroferrin is listed in Table IV, but crystallographic structural information is not available. EXAFS results for the diiron(III) form of methane monooxygenase have been recently reported,[56b] but more accurate data are needed before any sensible prediction of the value of $J$ can be made. The $-40$-$cm^{-1}$ value for the exchange-coupling interaction in uteroferrin is a lower limit from which an upper limit of $P = 1.88$ Å can be calculated. This value is somewhat at odds with the 1.98-Å value determined from EXAFS measurements. The latter value results in a calculated $J$ of only $-11$ $cm^{-1}$, suggesting the presence of a hydroxo bridge. A lower limit for $J$ of $-150$ $cm^{-1}$ for bovine spleen purple acid phosphatase has been reported.[10c] The calculated Fe–O(bridging) bond length of 1.776 Å is not comparable with the 1.98-Å EXAFS value. The presence of short, ~1.9-Å, Fe–O(tyrosine) distances, however, makes the EXAFS value less accurate.[10d]

## Conclusions

A quantitative relationship between the antiferromagnetic exchange interaction constant, $J$, and a single structural parameter $P$, the length of the shortest superexchange pathway, is presented. This correlation holds for multiply bridged dinuclear iron(III) complexes. It was also found that this relationship is valid for some oligonuclear complexes, thus allowing for their "magnetic dissection" into smaller, dinuclear units. On the basis of this relationship, data in the literature can be critically analyzed and, more importantly, structural and magnetic predictions can be made.

This relationship does not apply to singly bridged dinuclear iron(III) species. Calculations aimed at explaining this phenomenological correlation are in progress.[62]

**Acknowledgment.** This work received support in part from NIH Research Grant GM 32134 (to S.J.L.) from the National Institute of General Medical Services. We thank Professor Dr. K. Wieghardt for permission to quote data prior to publication and Drs. P. Turowski and R. Beer for reading the manuscript.

**Supplementary Material Available:** Figures S1–S3, describing correlations between the exchange-coupling interactions and various geometrical parameters for the diiron(III) complexes listed in Table I (3 pages). Ordering information is given on any current masthead page.

(62) Hart, J. R.; Rappe, A. K.; Gorun, S. M.; Upton, T. H. Submitted for publication.

Contribution from the Regional Sophisticated Instrumentation Centre, Indian Institute of Technology, Madras 600 036, India

# EPR and Structural Investigations on Single Crystals of $K_2NbO_2F_5 \cdot H_2O$

Ramakrishnan Geetha, Pillutla Sambasiva Rao, Varghese Babu, and Sankaran Subramanian*

*Received March 14, 1990*

The single-crystal structural investigation of dipotassium pentafluoroperoxoniobate hydrate, $K_2NbO_2F_5 \cdot H_2O$ (DPPN), is reported. The crystals are monoclinic with space group $C_2$, and the unit cell dimensions are $a = 8.927$ (4) Å, $b = 8.926$ (3) Å, $c = 9.266$ (2) Å, $\beta = 99.93$ (1)°, and $Z = 4$. The least-squares refinement of positional and anisotropic thermal parameters for all non-hydrogen atoms led to an $R$ factor of 0.057. The EPR spectra of a $\gamma$-irradiated single crystal of DPPN suggest a Nb hole species stable at room temperature. The anomalous behavior in spacing, number, and intensity of Nb hyperfine lines has been successfully explained by including a quadrupolar term in the Hamiltonian. The spin-Hamiltonian parameters for this hole species are as follows: $g_{xx} = 2.039$ (1), $g_{yy} = 2.013$ (1), $g_{zz} = 2.054$ (1); $A_{xx}(^{93}Nb) = 0.62$ (2), $A_{yy}(^{93}Nb) = 0.79$ (2), $A_{zz}(^{93}Nb) = 0.93$ (2) mT; $Q_{xx}(^{93}Nb) = Q_{yy}(^{93}Nb) = 0.065$, $Q_{zz}(^{93}Nb) = -0.130$ mT. The EPR results further indicate that the unpaired electron in the $[NbO_2F_5]^-$ radical occupies the nonbonding orbital of the peroxo oxygen atoms; this is further supported by EHMO calculations done on the precursor.

## Introduction

Reports of EPR investigations of the ions and complexes of the first-row transition series ($3d^n$) abound in the literature, while there have been relatively fewer reports on the second- ($4d^n$) and the third-row ($5d^n$) transition series. Only in the last two decades has there been considerable activity in the study of transition-metal complexes of second- and third-row transition-metal ions, especially those of Mo, Nb, Tc, Ru, Rh, Pd, and Pt, some for their biological significance[1] and others for their catalytic activity.[2] Whereas

* To whom correspondence should be addressed.

(1) Spiro, T. G., Ed. *Mo Enzymes*; Wiley-Interscience: New York, 1986; see also references therein.

0020-1669/91/1330-1630$02.50/0 

**Table I.** Details of Data Collection and Structure Refinement

| | | | |
|---|---|---|---|
| chem formula | $K_2NbO_2F_5 \cdot H_2O$ | $\rho_{calcd}$, g cm$^{-3}$ | 2.885 |
| fw | 316.0 | space group | $C2$ |
| cryst syst | monoclinic | temp, K | 298 |
| $a$, Å | 8.927 (4) | radiation | Mo K$\alpha$ |
| $b$, Å | 8.926 (3) | (graphite monochromatized) | |
| $c$, Å | 9.266 (2) | $\mu$(Mo K$\alpha$), cm$^{-1}$ | 0.71069 |
| $\beta$, deg | 99.93 (1) | no. of variables | 98 |
| $V$, Å$^3$ | 727.21 | $R_1$, $R_2$ | 0.057 |
| $Z$ | 4 | | |

the EPR spectra of 3d$^n$ complexes (some of them observed even at room temperature) are characterized (usually by well-resolved lines) with **g** tensors deviating only moderately from $g_e$ (with the exception of iron complexes under a strong tetragonal field yielding EPR spectra with effective $g$ factors ranging from 0 to 6[3]), the large spin–orbit interaction and short spin–lattice relaxation times found in 4d$^n$ and 5d$^n$ ions are responsible for the observation of EPR spectra of these ions mostly at low temperatures.[4] Only in cases where an orbital singlet lies much lower than any other state, is one likely to observe a spectrum above about 20 K. For example, a 4d$^3$ ion in an octahedral field, namely Tc(IV) in $K_2PtCl_6$, was detected at 77 K with $g = 2.050$.[5]

The stable peroxo–fluoro complexes of transition elements belong to groups IVa, Va, and VIa. Upon $\gamma$, X, or UV irradiation, the diamagnetic Nb(V) complexes become paramagnetic species, Nb(IV)[6-19] or Nb(VI),[20-22] which are stable below dry ice temperature (195 K). In this paper, a single-crystal X-ray investigation of dipotassium pentafluoroperoxoniobate hydrate (DPPN) is presented, along with the EPR results obtained for the paramagnetic centers produced in $\gamma$-irradiated DPPN single crystals. The EPR spectra are analyzed in terms of an appropriate spin Hamiltonian to evaluate the magnetic tensor parameters.

The deviation of geometry around the niobium ion from cubic symmetry as inferred from single-crystal EPR data has permitted the investigation of the effect of the nuclear quadrupole coupling constant on the splitting of the allowed transitions (vide infra). The quadrupole coupling constant obtained for $^{63}Cu$ nuclei, the most investigated paramagnetic probe, indicates that the data are sensitive enough to be a diagnostic tool for the determination of the stereochemical arrangement around the metal ion and of the nature of the ligands.[23] In addition to the data for copper, results concerning quadrupolar effects in EPR spectra of complexes are reported for gold,[24,25] vanadium,[26] molybdenum,[27] titanium,[28] and for cobalt.[29]

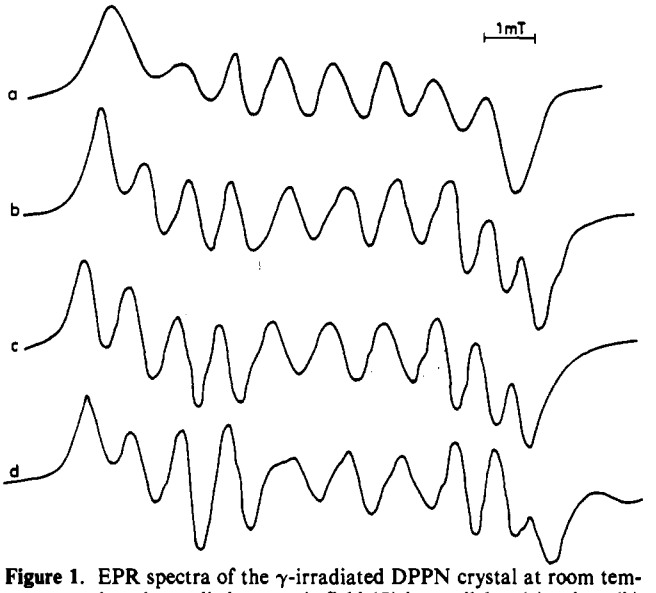


**Figure 1.** EPR spectra of the $\gamma$-irradiated DPPN crystal at room temperature when the applied magnetic field ($B$) is parallel to (a) axis $a$, (b) axis $b$, (c) axis $c^*$, and (d) 60° from axis $a$ in plane $ac^*$. Here, an eight-line pattern can be noticed when $B$ is parallel to axis $a$. Spectrum d indicates progressive decrease in the hyperfine coupling constant at both extremes, characteristic of strong quadrupolar perturbation (see text).

## Experimental Section

DPPN crystals were prepared according to the procedure of Vulectic and Djordjevic.[30] Niobium pentoxide was dissolved in 10 mL of 40% hydrofluoric acid by heating to 475 K in a platinum crucible. The solution was cooled and filtered, and 10 mL of 30% $H_2O_2$ was added. A stoichiometric amount of potassium hydroxide solution was added to the above solution. The resultant solution was cooled and then allowed to evaporate slowly. The crystals obtained were washed with alcohol and ether.

The compound was analyzed for potassium by means of atomic absorption using a Varian AA6D spectrometer, niobium by the tannin method, active oxygen by potassium permanganate titration, and fluoride by an ion-selective electrode.

Anal. Calcd: K, 24.7; Nb, 29.4; O(active), 5.1; F, 30.1. Found: K, 23.9; Nb, 29.9; O(active), 5.3; F, 30.5.

**Determination of Unit Cell Parameters.** Unit cell parameters were obtained by least-squares refinement of the $\theta$ values of 25 high-angle reflections. Three-dimensional intensity data were collected on an Enraf-Nonius CAD-4 single-crystal diffractometer. The details of data collection and structure refinement of DPPN single crystals are given in Table I. The space group was unambiguously identified as $C_2$ and not $C_m$ and $C_{2/m}$ as reported earlier by Grandjean and Weiss[31] on the basis of extinction results. With the measured dimensions of the crystal and a linear absorption coefficient of 2.605 mm$^{-1}$ for the crystal, the error in structure factor amplitude resulting from absorption was appreciable, and hence, an absorption correction was applied to the data in addition to the corrections for Lorentz and polarization effects.

The atomic scattering factors for Nb(V)[32] and for other non-hydrogen atoms[33] and the anomalous dispersion correction factors[34] are taken from the literature. The observed and calculated structure factors are given as supplementary material (Table S1). Calculations were carried out on

(2) Grasseli, R. K. *Surface Property and Catalysis by Non-Metals, Carbides, Sulphides and Other Transition Metal Complexes*; Reidel: Dordrecht, The Netherlands, 1983; pp 272–304.
(3) Sambasiva Rao, P.; Subramanian, S. *Mol. Phys.* **1985**, *54*, 415 and references therein.
(4) Wertz, J. E.; Bolton, J. R. *Electron Spin Resonance*; Chapman and Hall: New York, 1986; p 335.
(5) Low, W.; Llewellyn, P. M. *Phys. Rev.* **1958**, *110*, 842.
(6) Cozzi, D.; Vivarelli, S. *Z. Anorg. Allg. Chem.* **1955**, *279*, 165.
(7) Chester, P. F. *J. Appl. Phys.* **1961**, *32*, 866.
(8) Fedotov, V. N.; Garif'yanov, N. S.; Kozyrev, B. M. *Dokl. Akad. Nauk SSSR* **1962**, *145*, 1318.
(9) Edwards, P. R.; Subramanian, S.; Symons, M. C. R. *J. Chem. Soc. A* **1968**, 2985.
(10) Rasmussen, P. G.; Kuska, H. A.; Brubaker, C. H. *Inorg. Chem.* **1965**, *4*, 343.
(11) Lardon, M.; Gunthard, Hs. H. *J. Chem. Phys.* **1966**, *44*, 2010.
(12) Gainullin, I. F.; Ganif'yanov, N. S.; Kozyrev, B. M. *Dokl. Akad. Nauk SSSR* **1968**, *180*, 858.
(13) Labauze, G.; Samuel, E.; Livage, J. *Inorg. Chem.* **1980**, *19*, 1384.
(14) Attanasio, D.; Bellitto, C.; Flamini, A. *Inorg. Chem.* **1980**, *19*, 3419.
(15) Chu, K. C.; Kikuchi, C.; Viehmann, W. *J. Chem. Phys.* **1967**, *46*, 386.
(16) Abdulsalinov, R.; Livanova, L. P.; Mitrofanov, Yu. F.; Pol'skii, Yu. F.; Stepanov, V. G.; Falin, M. L. *Fiz. Tverd. Tela (Leningrad)* **1973**, *15*, 268.
(17) Hausmann, A.; Schreiber, P. *Solid State Commun.* **1972**, *10*, 957.
(18) Kiwi, J.; Suss, J. T.; Szapiro, S. *Chem. Phys. Lett.* **1984**, *106*, 135.
(19) Alexandrov, A. J.; Prokofiev, A. I.; Shishmentseva, E. V.; Evdokimova, T. F. *Dok. Akad. Nauk SSSR* **1985**, *284*, 1382.
(20) Shock, J. R.; Rogers, M. T. *Chem. Phys.* **1972**, *58*, 3856.
(21) Shock, J. R.; Rogers, M. T. *J. Magn. Reson.* **1975**, *19*, 303.
(22) Sweeney, K. L.; Halliburton, L. E. *Appl. Phys. Lett.* **1983**, *43*, 336.
(23) Childs, W. J.; Goodman, L. S. *Phys. Rev.* **1967**, *156*, 64.
(24) Van Willingen, H.; Van Rens, J. G. M. *Chem. Phys. Lett.* **1968**, *2*, 283.
(25) Belford, R. L.; Huang, D. T.; So, H. *Chem. Phys. Lett.* **1972**, *14*, 592.
(26) Madacsi, D. P.; Bartram, R. H.; Gilliam, O. R. *Phys. Rev. B* **1973**, *7*, 1817.
(27) Nilges, M. J.; Belford, R. L. *J. Magn. Reson.* **1979**, *35*, 259.
(28) Rinneberg, H.; Weil, J. A. *J. Chem. Phys.* **1972**, *56*, 2019.
(29) Chacko, V. P.; Manoharan, P. T. *J. Magn. Reson.* **1976**, *22*, 7.
(30) Vuletic, N.; Djordjevic, C. *J. Less-Common Met.* **1976**, *45*, 85.
(31) Grandjean, D.; Weiss, R. *Bull. Soc. Chim. Fr.* **1967**, *8*, 3040.
(32) Cromer, D. T.; Waber, J. T. *Acta Crystallogr.* **1965**, *18*, 104.
(33) Cromer, D. T.; Libermann, D. J. *Chem. Phys.* **1970**, *53*, 1891.
(34) Cromer, D. T.; Mann, J. B. *Acta Crystallogr.* **1968**, *A24*, 321.

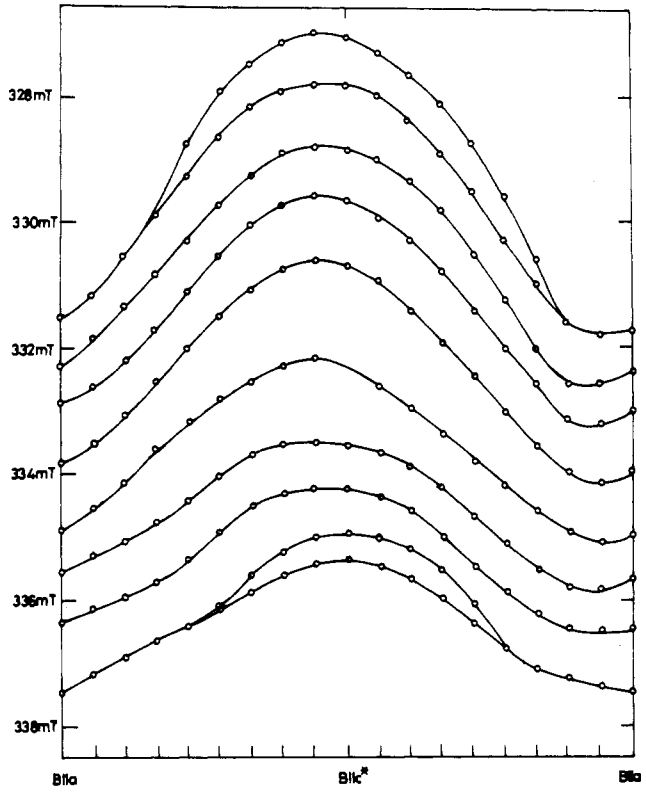


**Figure 2.** Isofrequency plot of the EPR spectra of the $\gamma$-irradiated DPPN crystal in the $ac^*$ plane at room temperature. One can notice an eight-line pattern when $B$ is parallel to the $a$ axis and a ten-line pattern when $B$ is parallel to $c^*$. In the $bc^*$ plane of rotation, a ten-line spectrum is observed throughout the plane whereas, in the $ab$ plane, the isofrequency plot is similar to Figure 2.

a Siemens 7580-E computing system using SHELX-76 and SHELX-86 crystallographic programs.[35]

**EPR Measurements.** Using a $^{60}$Co source, $\gamma$ irradiations of DPPN crystals were performed both at room temperature and at 77 K. The periods of irradiation were varied between 10 and 30 h, with a total dosage of 5–15 Mrads. The morphology of the crystal was determined prior to the experiment. The irradiated crystal was subsequently mounted onto a Varian E-229 goniometer device. The crystal rotations were performed about the three mutually perpendicular axes $a$, $b$, and $c^*$ ($c^*$ is perpendicular to $a$ and $b$) by using a Varian E-112 EPR spectrometer, and the spectra were recorded at each 10° interval. The room-temperature EPR spectra of $\gamma$-irradiated DPPN crystals for indicated orientations are shown in Figure 1, and an isofrequency plot in the $ac^*$ plane is shown in Figure 2. The isofrequency plots in the other two planes are given as supplementary material (Figures S1 and S2). The 10-line spectra (with line widths of 0.6 mT) are characteristic of an unpaired electron interacting with one $^{93}$Nb nucleus ($I = {}^9/_2$, 100%), although at some orientations only eight lines are apparent! The spectra clearly indicate anomalous intensities and hyperfine spacings. The bottom spectrum in Figure 1 shows progressive decrease in hyperfine coupling at both extremes, characteristic of strong quadrupolar perturbation. This second-order quadrupolar effect will be discussed later. The fluorine superhyperfine interaction was not observed even when the experiment was carried out at 77 K. Irradiation at 77 K followed by measurement at 77 K without warm-up gave EPR spectra identical with those obtained at room temperature. Variable-temperature work in the region 298–77 K did not show any significant change in the EPR spectra. The radicals decayed quite slowly and persisted for 4–5 days upon keeping the crystal at room temperature. When the crystal was heated in the EPR cavity, the radicals decayed very rapidly with a decrease in the line intensity, and complete annihilation of the radicals occurred around 350 K.

In order to derive the g tensor and the $^{93}$Nb hyperfine tensor, the angular variation of the center of gravity of the spectrum and the average hyperfine splitting were followed through the three orthogonal planes. To arrive at the principal values and direction cosines of $g$, both Schonland's procedure[36] and the least-squares procedure were adopted and found to yield identical results. Since $g$ is not isotropic, we used the variation of $g^2A^2$ to set up the hyperfine tensor and then derived the principal values of the A tensor and their direction cosines, using a 7580-E Siemens computing system. Simulations of the EPR spectra were performed with an IBM PC/XT.

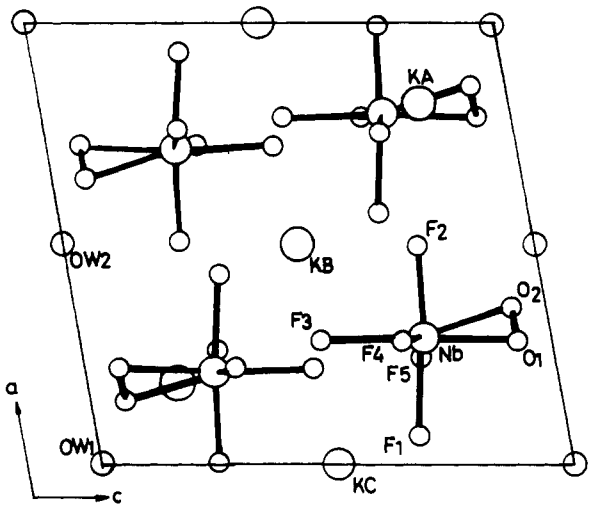


**Figure 3.** View of the unit cell of the DPPN crystal.

**Table II.** Fractional Atomic Parameters (×10$^4$) for Non-Hydrogen Atoms[a]

| atom | $x/a$ | $y/b$ | $z/c$ | occ |
|---|---|---|---|---|
| Nb | 2919 (1) | 5 (0) | 7266 (1) | 1.0 |
| $K_A$ | 8144 (2) | 4976 (1) | 8075 (2) | 1.0 |
| $K_B$ | 5 (0) | 7506 (1) | 5 (0) | 0.5 |
| $K_C$ | 0 (0) | 7486 (1) | 5 (0) | 0.5 |
| $F_1$ | 685 (8) | 5130 (3) | 6793 (9) | 1.0 |
| $F_3$ | 2814 (1) | 5192 (2) | 5142 (5) | 1.0 |
| $F_4$ | 2810 (4) | 7164 (5) | 6812 (2) | 1.0 |
| $F_2$ | 4970 (2) | 5794 (7) | 7512 (4) | 1.0 |
| $F_5$ | 2471 (2) | 2852 (2) | 7140 (2) | 1.0 |
| $O_1$ | 2813 (5) | 5372 (5) | 9254 (5) | 1.0 |
| $O_2$ | 3565 (0) | 3932 (0) | 9241 (0) | 1.0 |
| $OW_1$ | 000 (0) | 3426 (4) | 0 (0) | 0.5 |
| $OW_2$ | 5 (0) | 1948 (3) | 0 (0) | 0.5 |

[a] Standard deviation in the last digit is given in parentheses. The numbering of atoms is as shown in Figure 3.

## Results and Discussion

**(a) X-ray Results.** The unit cell dimensions of DPPN single crystals are given in Table I. The content of the unit cell is shown in Figure 3. The pentafluoroperoxoniobate anion has a heptacoordinated niobium atom. Positional parameters of all the atoms are listed in Table II, and important bond distances and bong angles are given as supplementary material (Table S2). The atoms $K_B$, $K_C$, and OW occupy special positions in the unit cell with 0.5 occupation number. The Nb–F and Nb–O bond distances ranging from 1.93 to 1.98 and 1.89 to 2.05 Å, respectively, correspond to metal–ligand single-bond distances. The peroxo oxygen bond distance of 1.45 Å agrees well with the bond distances found in other transition-metal peroxo complexes.[37,38] The anisotropic thermal parameters of atoms in the DPPN crystal are given as supplementary material (Table S3).

The favorable geometries for seven-coordination are the monocapped octahedron, the monocapped trigonal prism, and the pentagonal bipyramid. The interatomic distances play an important role in deciding the geometry prevalent in these monoperoxopentafluorometalates.

The displacements of atoms from the least-squares plane found in the unit cell were calculated and are given in the supplementary material (Table S4). From the least-squares planes present in the anion, it is evident that $O_2$ is not lying in the plane formed

(35) Sheldrick, G. M. SHELX-76: Program for Crystal Structure Determination. University of Cambridge, England, 1976.
(36) Schonland, D. S. *Proc. Phys. Soc.* **1959**, *73*, 788.
(37) Stomberg, R. *Acta Chem. Scand.* **1981**, *A35*, 389.
(38) Stomberg, R. *Acta Chem. Scand.* **1982**, *A36*, 423.

**Table III.** Spin-Hamiltonian Parameters of the γ-Irradiated DPPN System[a]

g Tensor

| principal values | direction cosines a | b | c* |
|---|---|---|---|
| $g_{xx}$ = 2.039 (1) | 0.846 | 0.482 | 0.227 |
| $g_{yy}$ = 2.013 (1) | −0.479 | 0.875 | −0.073 |
| $g_{zz}$ = 2.054 (1) | −0.234 | −0.046 | 0.971 |

A Tensor

| principal values, mT | direction cosines a | b | c* |
|---|---|---|---|
| $A_{xx}$ = 0.62 (2) | 0.980 | 0.127 | 0.155 |
| $A_{yy}$ = 0.79 (2) | −0.158 | 0.019 | 0.987 |
| $A_{zz}$ = 0.93 (2) | −0.123 | 0.991 | −0.030 |

Q Tensor

$Q_{xx} = Q_{yy} = 0.065$ mT $\quad Q_{zz} = -0.130$ mT

[a] A and Q tensors are for the $^{93}Nb$ nucleus.

**Table IV.** Direction Cosines of Various Bonds in $[NbO_2F_5]^{2-}$ Obtained from X-ray Data[a]

| bonds | direction cosines a | b | c* |
|---|---|---|---|
| Nb–$F_1$ | −0.974 | 0.060 | −0.022 |
| Nb–$F_2$ | 0.924 | 0.366 | 0.116 |
| Nb–$F_3$ | 0.125 | 0.088 | −0.988 |
| Nb–$F_4$ | 0.194 | −0.979 | 0.059 |
| Nb–$F_5$ | −0.013 | 0.978 | −0.209 |
| Nb–$O_1$ | −0.219 | 0.176 | 0.959 |
| Nb–$O_2$ | 0.127 | −0.464 | 0.877 |
| $O_2$–$O_1$ | −0.464 | 0.885 | −0.008 |
| Nb–($O_1$ + $O_2$)/2 | −0.042 | −0.168 | 0.985 |

[a] See Figure 3 for atom numbering.

by $F_3$, $F_4$, $F_5$, and $O_1$ and the geometry of the system is a monocapped octahedron. The niobium atom in the DPPN complex is displaced 0.18 Å from the equatorial plane formed by $F_3$, $F_4$, $F_5$, and $O_1$. Such a small displacement is usually observed for transition-metal peroxo compounds when, as in this case, the apical positions are occupied by identical groups. When the apical atoms are different or are differently coordinated, the central metal atom is, in most cases, displaced by 0.5 Å (Table 6 of ref 39). The crystal structure data for DPPN have contributed to a better understanding of the paramagnetic defects in these crystals (vide infra).

**(b) EPR Results.** The change in sign of the spin–orbit coupling constant as one goes from a less than half-filled to a greater than half-filled case leads to $g$ values <2.0023 ($g_e$) (electron-excess radicals) and >$g_e$ (hole species) respectively. Upon irradiation, it is reasonable to assume that the diamagnetic Nb(V) ion, which exists in a monocapped octahedral configuration, can be reduced to the Nb(IV) ion by trapping an electron. The resulting Nb(IV) species, which is expected to have $g_{eff} < g_e$, should show a large metal hyperfine splitting in the EPR spectrum, as envisaged by the previous reports on Nb(IV) compounds.[10-12,17,19] However, the EPR spectrum of DPPN, which spans a maximum of 10 mT with $g_{eff}$ 2.035 ($g_{eff} > g_e$), rules out the possibility of a Nb(IV) moiety in the present situation. On the other hand, the possible primary reaction could be the loss of an electron, which leads to a "hole"[40] in the highest occupied molecular orbital (HOMO), with the result that the unpaired electron is delocalized onto the nonbonding orbitals of the ligands and forms a stable "hole" species.

The spin Hamiltonian for the paramagnetic niobium system can be written, assuming orthorhombic **g**, **A**, and **Q** tensors and the nuclear Zeeman term.[41] The principal values and the direction cosines of the **g**, **A**, and **Q** tensors are listed in Table III. The atomic positional parameters, obtained from X-ray data (Table II), were utilized to determine the direction cosines of various bonds present in DPPN system and are given in Table IV. On comparison, it is observed that the direction cosines of one of the principal values of the **g** tensor, i.e., $g_{yy}$, coincide with that of the $O_2$–$O_1$ bond direction, the deviation being only 4.3°.

This result is rather surprising, as one would have expected the unique (or one of the) principal value(s) of the **g** tensor to lie along one of the Nb–ligand (either fluorine or oxygen) bond directions. In addition to this, the principal $g$ values are not in good agreement with the known systems of niobium(IV).[10-12,17,19] Hence, the possibility of the hole localized onto the peroxo oxygens leading to a superoxide ion like the paramagnetic species in the DPPN system is considered. Table V lists the **g** tensor and **A** tensor principal values of $O_2^-$ embedded in γ-irradiated zeolites measured at 77 K[42] and some of the reported Nb systems along with the currently investigated DPPN system. Here, the **g** tensor agreement between the present radical and $O_2^-$ is as good as that of the former with the known niobium systems, having a formally Nb(VI) oxidation state. The hyperfine values of the metal ions in zeolites are very small, similar to our case, whereas the hyperfine values in Nb(VI) systems deviate from our values. It is most likely, therefore, that the unpaired electron is localized mainly between the peroxo oxygen atoms and the small hyperfine interaction arises presumably via spin polarization of the niobium outer orbitals.

**Table V.** Magnetic Parameters for $[NbO_2F_5]^-$ and Related Species[a]

| system | g tensor | A tensor, mT | Q tensor, mT | ref |
|---|---|---|---|---|
| γ-irradiated AlHY zeolite | $g_{xx}$ = 2.009 | $A_{xx}$ = 0.48 | | 42 |
| | $g_{yy}$ = 2.003 | $A_{yy}$ = 0.57 | | |
| | $g_{zz}$ = 2.038 | $A_{zz}$ = 0.65 | | |
| γ-irradiated ScY zeolite | $g_{xx}$ = 2.009 | $A_{xx}$ = 0.44 | | 42 |
| | $g_{yy}$ = 2.002 | $A_{yy}$ = 0.51 | | |
| | $g_{zz}$ = 2.030 | $A_{zz}$ = 0.57 | | |
| γ-irradiated LaY zeolite | $g_{xx}$ = 2.009 | $A_{xx}$ = 0.90 | | 42 |
| | $g_{yy}$ = 2.005 | $A_{yy}$ = 0.80 | | |
| | $g_{zz}$ = 2.044 | $A_{zz}$ = 1.20 | | |
| $[NbO_4]^{2-}$ | $g_{xx}$ = 2.021 | $A_{xx}$ = −2.79 | | 9 |
| | $g_{yy}$ = 2.021 | $A_{yy}$ = −2.79 | | |
| | $g_{zz}$ = 2.025 | $A_{zz}$ = −2.70 | | |
| $[NbOF_5]^-$ | $g_{av}$ = 2.022 | $A_{av}$ = 0.21 | | 21 |
| Nb(II) doped in $CaWO_4$ | $g_{xx}$ = 2.013 | $A_{xx}$ = 2.70 | $Q_{zz}$ = +0.046 | 16 |
| | $g_{yy}$ = 2.008 | $A_{yy}$ = 2.51 | $Q_{yy}$ = −0.028 | |
| | $g_{zz}$ = 2.053 | $A_{zz}$ = 2.95 | $Q_{xx}$ = −0.019 | |
| $[NbO_2F_5]^-$ | $g_{xx}$ = 2.039 | $A_{xx}$ = 0.62 | $Q_{zz}$ = −0.130 | present |
| | $g_{yy}$ = 2.013 | $A_{yy}$ = 0.79 | $Q_{xx}$ = 0.065 | work |
| | $g_{zz}$ = 2.054 | $A_{zz}$ = 0.93 | $Q_{yy}$ = 0.065 | |

[a] The hyperfine values are for Al, Sc, and La, respectively, for the AlHY, ScY, and LaY zeolites.

To proceed further, we now turn to an examination of the $^{93}Nb$ hyperfine tensor. The metal hyperfine interaction is considered to originate at the niobium nucleus. Comparison of the direction cosines of the **A** tensor (Table III) with Table IV shows that $A_{yy}$, one of the hyperfine principal values, lies close to the Nb–$O_1$ bond direction. The angle between $A_{yy}$ and the Nb–$O_1$ bond direction is ~10.1°. The **A** tensor consists of an isotropic part (equivalent to 0.78 mT) and an anisotropic part. The isotropic part of the hyperfine tensor must arise largely from an unpaired electron density in the niobium 5s orbitals from spin polarization of the ($O_1$–$O_2$)–Nb bond. Using the value $A_{iso}(^{93}Nb,5s)$ = 155.0 mT,[9] we obtain $f(^{93}Nb,5s)$ = 0.5%. As mentioned earlier in our **g** tensor discussion, this small spin density on the niobium ion confirms that the radical $[NbO_2F_5]^-$ produced in the DPPN system is very similar to the $O_2^-$ ion and is responsible for the observed EPR spectra. Also, as can be seen from Tabler IV, the fact that one

(39) Larking, I.; Stomberg, R. *Acta Chem. Scand.* **1971**, *25*, 898.
(40) Atkins, P. W.; Symons, M. C. R. *The Structure of Inorganic Radicals*; Elsevier: Amsterdam, 1967.
(41) Abragam, A.; Bleaney, B. *Electron Paramagnetic Resonance of Transition Ions*; Clarendon Press: Oxford, England, 1970.
(42) Wang, K. M.; Lunsford, J. H. *J. Phys. Chem.* **1971**, *75*, 1165.
(43) Attanasio, D.; Bellitto, C.; Flamini, A.; Pennesi, G. *Chem. Phys. Lett.* **1980**, *72*, 307.

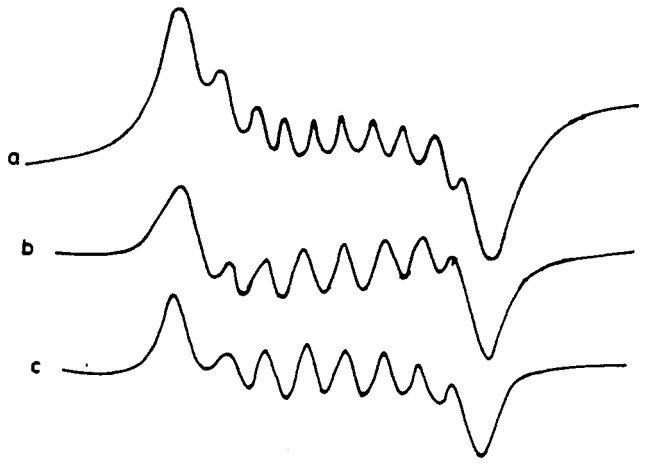


**Figure 4.** Simulation of the EPR spectra (using the parameters given in Table III) when $B$ is parallel to the $a$ axis: (a) without $Q$ inclusion and (b) with $Q$ inclusion. Trace c is the experimental spectrum.

of the principal values of the A tensor is along the Nb–$O_1$ and not along the Nb–F bond direction further supports the idea that the radical formed is very similar to the $O_2^-$ ion. The small hyperfine values found for Al, Sc, and La in zeolites[42] indicate approximately 0.5–1.0% of spin density on the respective metal ions, comparable to 0.5% obtained for Nb.

The anisotropic hyperfine tensor components are −0.16, 0.01, and 0.15 mT, respectively. These components are within the line widths of the EPR spectra and will not give any fruitful information on analysis. As the hyperfine coupling constants of $^{93}$Nb are low and unpaired spin density on $^{93}$Nb is 0.5%, the spin density transfer onto the $^{19}$F ligands is negligible. This fact is responsible for the absence of $^{19}$F superhyperfine interaction in the γ-irradiated DPPN system.

The EPR spectrum of γ-irradiated DPPN does not show equal spacings and intensities of Nb hyperfine lines. Since the hyperfine coupling is 0.78 mT, even a second-order hyperfine interaction contribution would not explain this behavior. Further, the observation of decets for $B \parallel b$ and $c^*$ is quite easy to analyze, while an eight-line pattern for $B \parallel a$ will require additional terms such as the nuclear quadrupole coupling constant and nuclear Zeeman interaction in the spin Hamiltonian to explain the phenomena satisfactorily. This has been verified by simulating the EPR spectrum with and without quadrupole interaction terms for the conditions $B \parallel a$, $b$, and $c^*$. The principal values of the **g**, **A**, and **Q** tensors given in Table III have been used for the spectral simulation, by using a Lorentzian line shape and a peak-to-peak width of 0.5 mT. A typical simulated spectrum, when $B$ is parallel to the $a$ axis, is shown in Figure 4. The effect of quadrupole interaction is very clear from this figure; an eight-line pattern is observed by including these terms and a ten-line spectrum is seen when the interaction terms are neglected. The agreement between the theoretical and experimental spectra is quite good, confirming the influence of quadrupole interaction.

From the quadrupole coupling tensor **Q**, the $e^2qQ$ value is calculated for the niobium nucleus by using the equation

$$e^2qQ = \{[4I(2I - 1)]/3\}Q_{zz} \quad (1)$$

and is given in Table VI along with the earlier reported values of $e^2qQ$ in other related niobium compounds. The monocapped octahedral geometry in the DPPN crystal also displays high quadrupole coupling constant for the $^{93}$Nb nucleus as against other systems known in the literature. A similar observation is seen in the case of copper complexes where sulfur ligands display low quadrupole coupling constants whereas oxygen ligands show characteristic high quadrupole coupling constants.[44] Further, it is known that octahedral and tetrahedral sites display large quadrupole coupling constants and four-coordinate square-planar sites show small values with respect to copper systems. Thus, correlation with geometry seems quite strong with respect to $Q$ values and there are subtler correlations with ligand electronic structure.[45] Hence, this system is one of the unique cases that show large quadrupole coupling interaction of niobium at ambient temperatures.

**Table VI.** $^{93}$Nb Quadrupole Coupling Constant Data[a]

| compd | temp, K | $e^2qQ$, MHz | method | ref |
|---|---|---|---|---|
| $NbCl_5$ | 298 | 78.26 | NQR | 27 |
| $KNbO_3$ | 77 | 16.0 | NQR | 28 |
| $LiNbO_3$ | 298 | 22.0 | NQR | 29 |
| $NbF_5$ | 298 | 114.63 ($\eta$ = 0.137) | NQR | 43 |
| $NbBr_5$ | 298 | 59.71 ($\eta$ = 0.454) | NQR | 43 |
| $NbOCl_3$ | 298 | 109.69 ($\eta$ = 0.334) | NQR | 43 |
| $[NbO_2F_5]^-$ | 298 | 177.4 ($\eta$ = 0.0) | EPR | present work |

[a] $\eta$ = asymmetry parameter $(Q_{xx} - Q_{yy})/Q_{zz}$.

With reference to the stereoscopic view of the unit cell, though four molecules per unit cell are present in monoclinic DPPN crystals, the absence of different sites in EPR spectra suggests that the paramagnetic centers are magnetically almost equivalent within the line width. In other words, the two different sites in the DPPN system (space group $C2$) are not resolved due to possible librational modes of the Nb center in γ-irradiated DPPN crystals at room temperature, which lead to magnetically equivalent sites. The different sites would perhaps be resolved (from X-ray data: two sites for $a$- and $c^*$-axis rotation and one site for $b$-axis rotation) if the EPR spectra were recorded below 77 K.

It may be argued that the anomalous hyperfine pattern observed in the $ac^*$ or $ab$ plane of rotation may be (a) due to the overlap of different sites that could not be resolved at room temperature or at 77 K, (b) due to the effects of line width dependence on $m_I$, or (c) due to unresolved hyperfine interaction. However, our confidence that this anomalous hyperfine pattern, i.e., especially the eight-line pattern, is indeed due to quadrupolar interaction stems from the fact that even when the applied magnetic field is parallel to one of the crystallographic axes, i.e. the $a$ axis, where the Nb sites are magnetically equivalent, an eight-line hyperfine pattern is seen, which could be reproduced only by the inclusion of quadrupolar terms in the Hamiltonian.

**(c) EHMO Results.** Semiempirical molecular orbital calculations can be used to describe the various energy levels present in the system and to rationalize the experimental observation based on the molecular orbital diagram. The EHMO calculations were performed on the $[NbO_2F_5]^{2-}$ system with the ICON-8 program[46] running on the Siemens 7580-E computer. The input parameters (given as supplementary material, Table S5) used in the program consist of precise atomic coordinates of various atoms (available from crystal structure data), the Slater orbital exponents (STO's), and the corresponding valence-state ionization energies (VSIE's). The STO's and VSIE's for Nb (5s 1.90, −10.10; 5p 1.85, −6.86, 4d 4.08, −12.10) are taken from ref 47. The molecular orbital energy diagram obtained from EHMO calculations is given in Figure 5. From the coefficients of atomic orbitals representing the resultant molecular orbitals in the DPPN system, the "HOMO" in the DPPN crystal is ascertained to be the nonbonding orbital of the peroxo oxygen atoms:

$$\Psi_{HOMO} = 0.5875p_x(O_1) + 0.3210p_y(O_1) + 0.2480p_z(O_1) - 0.6094p_x(O_2) - 0.3280p_y(O_2) - 0.2885p_z(O_2)$$

where $O_1$ and $O_2$ are the peroxo oxygen atoms of the DPPN system. Thus, the hole is created entirely on the oxygen atoms of the DPPN crystal. The molecular orbital calculations explain the reason for the similarity between the $[NbO_2F_5]^-$ radical and

(44) White, L. K.; Belford, R. L. *J. Am. Chem. Soc.* **1976**, *98*, 4428.

(45) White, L. K.; Belford, R. L. *Chem. Phys. Lett.* **1976**, *37*, 553.
(46) Summerville, R. H.; Hoffmann, R. *J. Am. Chem. Soc.* **1976**, *98*, 7240.
(47) Whangbo, M. H.; Foscher, F. *Inorg. Chem.* **1981**, *20*, 113.

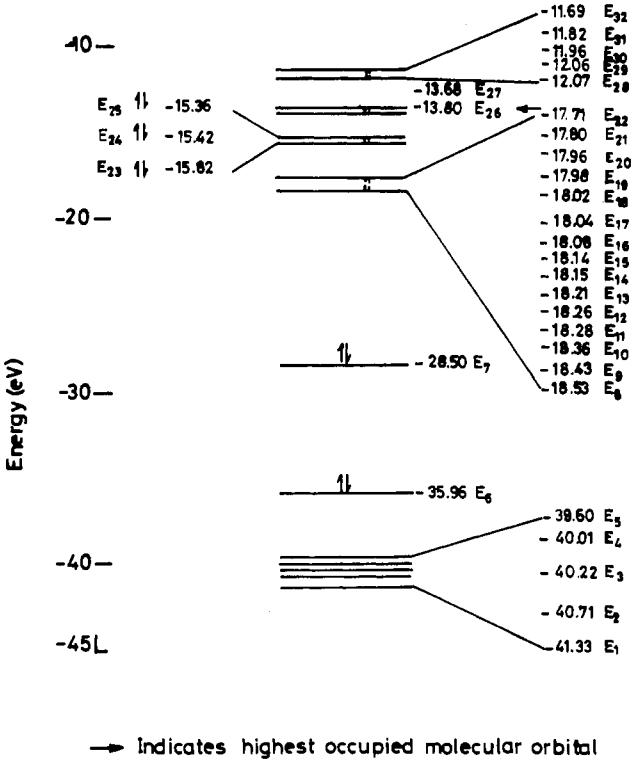


**Figure 5.** Energy level diagram of the $[NbO_2F_5]^{2-}$ ion. The arrow indicates the highest occupied molecular orbital, coefficients for which are given in the text.

the $O_2^-$ ion and the fact that one of the principal values of the g tensor lies along the $O_1$–$O_2$ bond direction.

## Conclusions

The present work on the DPPN X-ray structure has removed the existing ambiguity about its previously reported space group and confirmed it to be *C*2. The stability and observability of the $[NbO_2F_5]^-$ species at room temperature are quite interesting, while most of the Nb species like the $[NbOF_5]^-$ hole species are observable only below 195 K. A reduction in symmetry from $O_h$ to $C_{2v}$, which resulted in the unpaired electron occupying a nondegenerate nonbonding MO, is probably the reason that the radical could give an observable spectrum at room temperature. In other words, the "hole" is almost exclusively shared by the peroxo oxygen atoms, as in the superoxide $O_2^-$ ion. The present paramagnetic center could not have been observed at room temperature if the hole were localized fully on the central metal atom, i.e. on Nb, converting the Nb(V) into Nb(VI). Hence, the presence of the peroxo ligand has helped in the stability and identification of the radical at room temperature. The above reasoning is further supported by the EHMO calculations done on the DPPN system.

The small $^{93}Nb$ hyperfine coupling constant arises via spin polarization of the ($O_1$–$O_2$)–Nb bond. The pertubation due to quadrupole interaction has been inferred via its effect on the allowed transitions. The forbidden transitions are weak and unresolved due to the large inherent line widths. ENDOR experiments on the DPPN system will be useful in understanding the nature of the interaction present and in independently obtaining the quadrupolar coupling constants. Also, the EPR spectra below 77 K might lead to the resolution of different sites and throw further light upon the niobium center present in the system, but this could not be done due to lack of facilities.

**Acknowledgment.** R.G. thanks the IIT, Madras, for allowing her to pursue research on a part-time basis. P.S.R. thanks the CSIR, India, for a fellowship.

**Registry No.** DPPN, 12357-41-4; $[NbO_2F_5]^-$, 31727-99-8.

**Supplementary Material Available:** Isofrequency plots in *bc** and *ab* planes (Figures S1 and S2), bond distances and bond angles in $[NbO_2F_5]^{2-}$ (Table S2), anisotropic temperature factors for atoms in DPPN (Table S3), least-squares planes of the anion (Table S4), and input parameters for EHMO calculations on the $[NbO_2F_5]^{2-}$ system (Table S5) (6 pages); observed and calculated structure factors for DPPN (Table S1) (5 pages). Ordering information is given on any current masthead page.

---

Contribution from the Department of Chemistry, University of Otago, P.O. Box 56, Dunedin, New Zealand

# Reactions of Coordinated Imidazole. Oxidation Products and Ring Cleavage in the Reactions of $RImH^{3+}$ (R = $(NH_3)_5Co$) with $CH_3COOBr$ and HOBr

Allan G. Blackman, David A. Buckingham,* Charles R. Clark, and Jim Simpson

*Received August 27, 1990*

Treatment of $RImH^{3+}$ (R = $(NH_3)_5Co$, ImH = imidazole) with aqueous $Br_2$ in acetate (or phosphate) buffer at pH 4–6 results in R(parabanate)$^{2+}$ (**2**) as the only product (parabanic acid = imidazolidine-2,4,5-trione). A crystal structure of [R(parabanate)]$Cl_2 \cdot 3H_2O$ (orthohombic, $P2_12_12_1$; $a$ = 6.936 (1), $b$ = 11.032 (3), $c$ = 19.652 (3) Å; $Z$ = 4; $R$ = 0.0491, 1301 reflections) is reported. Formation of **2** appears to occur via initial reaction with $Br_2$(aq) to give R4,5-$Br_2ImH^{3+}$ and R2,4,5-$Br_3Im^{2+}$ (**1**), followed by further bromination at C-2 by AcOBr to give a tetrabromo species (**4**), which rapidly hydrolyses. The same product results from oxidation by $Cl_2$(aq) in the absence of acetate buffer. Treatment of $RImH^{3+}$ with HOBr in aqueous solution results in three main products. These were identified as R$(C_2N_2H_3O_2)^{2+}$ (**7**) containing (probably) the N-coordinated conjugate base of dioxamide, R$(CHO)_2^{2+}$ (**11**) containing the N-coordinated conjugate base of diformamide, and R$(C_3N_2O_3H_3)^{2+}$ (**12**) containing N-coordinated 2-hydroxyimidazolidine-4,5-dione. A crystal structure of [R(2-hydroxyimidazolidine-4,5-dione)]$(CF_3SO_3)_2$ (monoclinic, $C2/m$; $a$ = 32.325 (20), $b$ = 8.037 (4), $c$ = 7.195 (5) Å; $\beta$ = 91.92 (5)°; $Z$ = 4; $R$ = 0.0951, 1348 reflections) is reported.

## Introduction

The present experiments arose out of attempts to define the reaction sequence when $RImH^{3+}$ (R = $(NH_3)_5Co$) is treated with $Br_2$ in aqueous solution.[1] When the reaction is carried out under reasonably acidic conditions ([$H^+$] ≥ 0.01 M), one of the products, R2,4,5-$Br_3ImH^{3+}$ (**1**) loses (slowly) its imidazole ligand by hy-

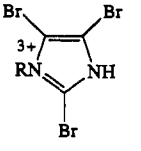


**1**

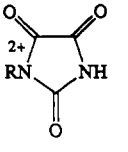


**2**

(1) All three sites are successively brominated according to the scheme $RImH^{3+} \rightarrow$ R4-$BrImH^{3+} \rightarrow$ R4,5-$Br_2ImH^{3+} \rightarrow$ R2,4,5-$Br_3ImH^{3+}$; cf.: Blackman, A. G.; Buckingham, D. A.; Clark, C. R.; Kulkarni, S. *Aust. J. Chem.* **1986**, *39*, 1465. See also: Blackman, A. G.; Buckingham, D. A.; Clark, C. R. *J. Am. Chem. Soc.*, in press.

0020-1669/91/1330-1635$02.50/0 